Blinking Mechanisms and Intrinsic Quantum-Confined Stark Effect in Single Methylammonium Lead Bromide Perovskite Quantum Dots

Xue Han, Guofeng Zhang,* Bin Li, Changgang Yang, Wenli Guo, Xiuqing Bai, Peng Huang, Ruiyun Chen, Chengbing Qin, Jianyong Hu, Yifei Ma, Haizheng Zhong, Liantuan Xiao,* and Suotang Jia

Lead halide perovskite quantum dots (QDs) are promising materials for next-generation photoelectric devices because of their low preparation costs and excellent optoelectronic properties. In this study, the blinking mechanisms and the intrinsic quantum-confined Stark effect (IQCSE) in single organic–inorganic hybrid $CH_3NH_3PbBr_3$ perovskite QDs using single-dot photoluminescence (PL) spectroscopy is investigated. The PL quantum yield-recombination rates distribution map allows the identification of different PL blinking mechanisms and their respective contributions to the PL emission behavior. A strong correlation between the excitation power and the blinking mechanisms is reported. Most single QDs exhibit band-edge carrier blinking under a low excitation photon fluence. While under a high excitation photon fluence, different proportions of Auger-blinking emerge in their PL intensity trajectories. In particular, significant IQCSEs in the QDs that exhibit more pronounced Auger-blinking are observed. Based on these findings, an Auger-induced IQCSE model to explain the observed IQCSE phenomena is observed.

X. Han, Prof. G. Zhang, Dr. B. Li, C. Yang, W. Guo, X. Bai, Dr. R. Chen, Dr. C. Qin, Dr. J. Hu, Dr. Y. Ma, Prof. L. Xiao, Prof. S. Jia
State Key Laboratory of Quantum Optics and Quantum Optics Devices
Institute of Laser Spectroscopy
Collaborative Innovation Center of Extreme Optics
Shanxi University
Taiyuan 030006, China
E-mail: guofeng.zhang@sxu.edu.cn; xlt@sxu.edu.cn

Dr. B. Li
Key Laboratory of Spectral Measurement and Analysis
of Shanxi Province
College of Physics and Information Engineering
Shanxi Normal University
Linfen 041004, China

P. Huang, Prof. H. Zhong
Beijing Key Laboratory of Nanophotonics and Ultrafine Optoelectronic
Systems
School of Materials Science & Engineering
Beijing Institute of Technology
Beijing 100081, China

1. Introduction

Lead halide perovskite quantum dots (QDs) received considerable attention in recent years, because of their unique optoelectronic properties such as high photoluminescence (PL) quantum yields (QYs), large absorption coefficient, fast exciton generation and slow exciton recombination, and high tolerance to structural defects and surface states.[1,2] Their application prospects include photovoltaics, light-emitting diodes, lasers, photodetectors, and single-photon sources.[3–12] Despite these advantages, PL blinking occurs in perovskite QDs, compromising the performance of PL-based applications.[13–15] PL blinking refers to the intensity intermittency between bright (on) and dim/dark (off) states with time.[16–18] Non-radiative Auger recombination and surface trap-induced non-radiative recombination are the two models for explaining this phenomenon. The previous reports attributed nonradiative Auger recombination as the major cause of the PL blinking behavior of perovskite QDs.[19] In this model, PL blinking originates from the charging and discharging processes in the QDs. The radiative recombination of excitons dominates the bright emission state of the QD. Once the QD is ionized, a charged state is formed in the QD. The charged state can initiate efficient nonradiative Auger recombination process, thereby quenching the PL emission via passing the exciton energy to a third carrier (either electron or hole).[20,21] The QD switches between the neutral and charged states, causing PL blinking. This type of blinking is termed as Auger-blinking. On the other aspect, surface trap-induced nonradiative recombination was believed to play a major part in the PL blinking of perovskite QDs.[3,22,23] Although the optical and electronic properties of perovskites materials are highly tolerant to structural defects and surface states,[2] there are also shallow surface traps in the perovskite QDs, also called multiple recombination centers (MRCs),[24] which provide nonradiative channels for band-edge carriers.[23,25]

The random activation and deactivation of MRCs cause a constantly changing nonradiative recombination rate and hence cause PL blinking. This type of blinking is known as band-edge carrier (BC)-blinking.[26] The coexistence of Auger- and BC-blinking in single perovskite QDs have also been reported.[25,27] The fluorescence lifetime-intensity distribution (FLID) and the scaling of radiative rates are regarded as common and effective experimental methods applied for investigating the PL blinking mechanisms in QDs.[23,25,28] However, when two types of blinking coexist in one QD, it becomes challenging to determine the blinking mechanisms and their respective contributions to the PL emission.

Besides blinking, perovskite QDs exhibit spectral diffusion with random changes in their emission spectra over time,[29,30] which is another challenge for the QD-based applications. The spectral diffusion is due to energetic shifts induced by intrinsic quantum-confined Stark effect (IQCSE).[31,32] The IQCSE refers to the change of the energy band structure of QDs under the action of a local electric field around the QDs,[33] of which a discrete hopping of surface charges generates the local electric field.[34–36] The surface charges hopping between different surface-trap sites or fluctuating within the ligand layer result in the spectral shifting in time.[32,37] At room temperature, the spectral diffusion results in broadening in the ensemble emission spectrum, compromising the color-purity of optoelectronic devices. Investigation of the origin of IQCSE helps to understand and suppress the spectral broadening behavior. However, the IQCSE is often obscured in ensemble measurements at room temperature. Both the IQCSE and the blinking mechanisms involve the extra charges, nevertheless, their potential connection lacks experimental investigation so far.

Most of the previous reports on PL blinking and IQCSE focused on inorganic $CsPbX_3$ (X = Cl, Br, I)[3,19,22,23] and CdSe-based QDs,[31,32,38,39] respectively. Compared with those QDs, organic–inorganic hybrid perovskite QDs have many unique properties, including a significantly longer carrier lifetime,[40] enhanced two-photon absorption properties,[41] and a slower bi-exciton Auger recombination rate.[42] These properties make the hybrid perovskite QD an ideal candidate in high-quality optoelectronic devices. Investigating the blinking mechanisms and the IQCSE of organic–inorganic perovskite QDs at the single-particle level can provide a deeper understanding of their fundamental properties and functionalities, and it is, therefore, essential for unleashing the materials' full application potentials.

In this study, we investigated the blinking mechanisms and the IQCSE in single $CH_3NH_3PbBr_3$ perovskite QDs by employing time-tagged, time-resolved, and time-correlated single-photon counting (TTTR-TCSPC) technique.[43,44] This technique effectively extracts the information of the blinking mechanisms and the IQCSE from the PL intensity trajectories, decay curves, second-order correlation function ($g^{(2)}$) curves, and FLID maps. Also, the PLQY-recombination rate distribution (PQRD) map is developed to effectively distinguish the blinking mechanisms in single perovskite QDs. The single-dot PL spectroscopy at room temperature reveals the origin of IQCSE to correlate with the Auger processes.

2. Results and Discussion

2.1. Optical Properties of Single $CH_3NH_3PbBr_3$ QDs

The preparation of $CH_3NH_3PbBr_3$ perovskite QDs was based on the emulsion synthesis method,[45] which results in monodisperse QDs with tunable sizes. The QDs have a diameter of 3.2 ± 0.8 nm, measured from the transmission electron microscopy (TEM) image (**Figure 1**a). The absorption and PL emission spectra of the QDs in toluene are presented in Figure 1b. The PL spectrum centers at 472 nm with a full width at half-maximum of 20 nm. By covering the QDs with a protective polymer layer, the QDs are stable enough to achieve repeatable single-dot measurements. The confocal scanning PL image in Figure 1c shows that the QDs have a uniform dispersion on the glass substrate. The color change in the PL image from blue to red indicates an increase in the PL intensity. It is worth mentioning that aggregates appeared alongside the single QDs in this image as well, and a fast recognition method has been used to distinguish single QD from aggregates during measurement, as demonstrated in our previous report.[43,46] The average number of photons absorbed per QD per pulse, $<N>$, was determined as $<N> = j_{exc}\ \sigma$, where j_{exc} is the per-pulse photon fluence, and σ is the QD absorption cross-section.[47] The average σ is 9×10^{-16} cm², as shown in Figure 1d, which is in good agreement with the previous reports.[47,48] Detailed experimental methods for the determination of $<N>$ and σ are provided in Supporting Information.

2.2. Blinking Mechanisms of Single QDs

We investigated the blinking mechanisms of single $CH_3NH_3PbBr_3$ perovskite QDs using the single-dot PL spectroscopy at two different excitation conditions: (1) a low excitation photon of fluence of $<N> = 0.04$; and (2) a high excitation photon fluence of $<N> = 0.24$. **Figure 2**a presents a typical PL intensity trajectory obtained under the low excitation fluence. The corresponding PL intensity histogram is shown on the right panel. Under this excitation condition, the PL trajectories of the most single QDs show a stable bright-state, accompanied by rare PL blinking events. The corresponding FLID map is obtained by mono-exponential fitting of each time bin of 10 ms for the PL trajectory (Figure 2d). The FLID, as an experimental data analysis method, is a distribution map obtained by combining PL lifetime and intensity to reveal the blinking mechanisms of QDs through different distribution characteristics.[23,25,26] However, this FLID is challenging to distinguish the blinking mechanisms of the QD due to the small probability of occurrence of gray and dim states in FLID. Therefore, here we combine it with the scaling of radiative rates to determine the blinking mechanisms. Figure 2g presents two typical PL decay curves obtained from bright- and dim-state PL regions ($I_1 = 79$ counts/10 ms, $I_2 = 21$ counts/10 ms, and the background noise is 1 count /10 ms) marked in respective colors on intensity histograms of Figure 2a. They are fitted well by single-exponential functions with lifetimes of 14.85 ns (τ_1) and 3.94 ns (τ_2), respectively. Here, we normalize the PLQY by setting that of the highest intensity level (Q^{max}) in the PL intensity time trace as
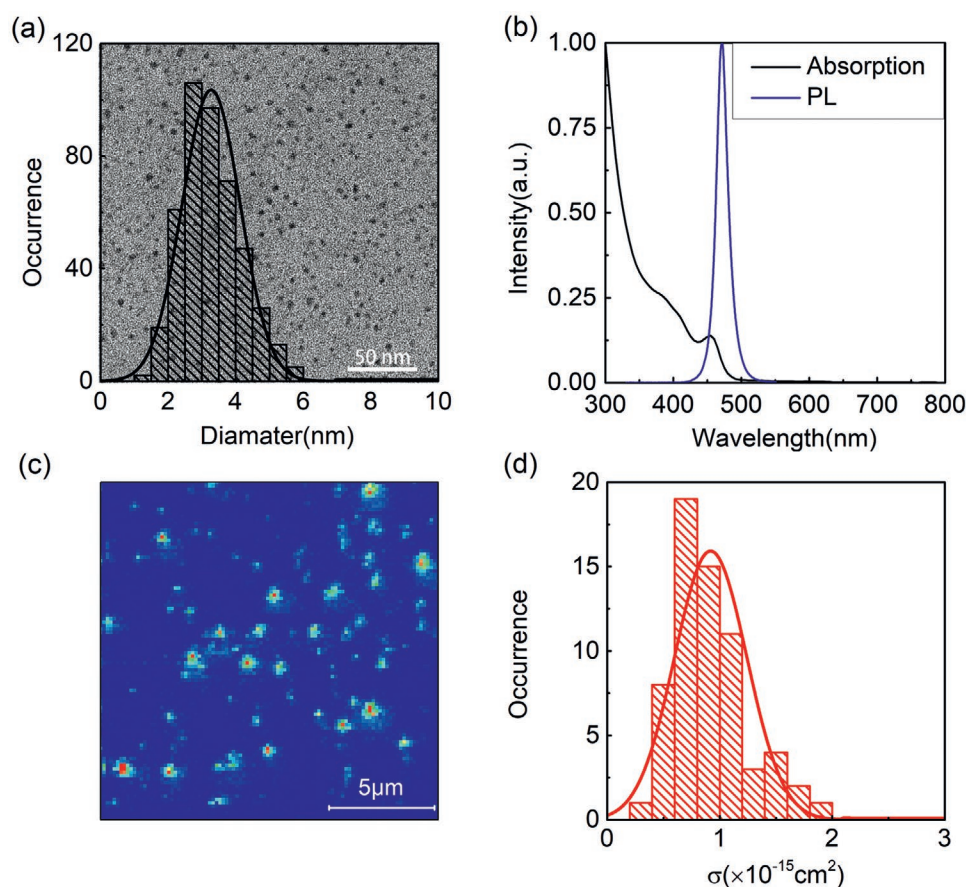
**ADVANCED
SCIENCE NEWS**

www.advancedsciencenews.com

**NANO · MICRO
small**

www.small-journal.com

Figure 1. a) TEM image and size distribution of $CH_3NH_3PbBr_3$ perovskite QDs. b) Absorption and PL spectra of $CH_3NH_3PbBr_3$ QDs dispersed in toluene. c) Confocal scanning PL image of $CH_3NH_3PbBr_3$ perovskite QDs deposited on a glass substrate. d) Histogram of the absorption cross-sections (σ) of single $CH_3NH_3PbBr_3$ perovskite QDs.

a unity,[49] so the normalized PLQY of other intensity levels can be expressed as $Q = I/I^{max}$. By combining $Q = k_r/(k_r + k_{nr}) = k_r\tau$, the scaling of radiative rates of the dim state (k_{r2}) and the bright state (k_{r1}) can be calculated as

$$\frac{k_{r2}}{k_{r1}} = \frac{I_2}{I_1} \times \frac{\tau_1}{\tau_2} = \frac{21-1(\text{background})}{79-1(\text{background})} \times \frac{14.85}{3.94} \approx 0.97 \quad (1)$$

The scaling of 0.97 is close to 1.0, which is evidence of BC-blinking.[26] We found that ≈92% of QDs show BC-blinking under the low excitation of $<N> = 0.04$. The remaining cases (≈8%) are found to deviate from the BC-blinking.

As the excitation increases to $<N> = 0.24$, the blinking behavior of the same QD is obviously intensified, showing more frequent PL intensity intermittencies in Figure 2b. The corresponding PL intensity histogram in the right panel displays an obvious two-state distribution. The corresponding FLID map partly deviates from a linear dependence (Figure 2e), implying that the blinking behavior deviates from the BC-blinking under the high-power excitation.[23] Fitting PL decay curves in Figure 2h, the scaling of radiative rates are calculated to be 1.35 (see Supporting Information), significantly above that of BC-blinking. The scaling value is also notably smaller than

that for the Auger-blinking between trion and exciton states, which is 2.[26,50] The curvature of the FLID and the deviations of the scaling indicate that Auger-blinking also occurs in addition to the BC-blinking in the QD under the high-power excitation. ≈38% of single QDs are this case at $<N> = 0.24$. The remaining QDs (≈62%) seem to still be BC-blinking, for example, the QD possesses the nearly linear FLID and the radiative rates scaling of 0.97 (see Supporting Information for details), as shown in Figure 2c,f,i. Nonetheless, just from the FLID and the scaling of radiative rates, we could not determine the exact proportion of the blinking mechanisms.

2.3. The Method of PLQY-Recombination Rate Distribution (PQRD) Map

Here, we propose the use of PQRD map to determine the origin of PL blinking and to distinguish possibly different blinking mechanisms with a reliable assessment on their proportions. The PQRD map is obtained by calculating the recombination rates (k, k_r, or k_{nr}) as a function of the normalized PLQY (Q/Q^{max}) (see Supporting Information for details). **Figure 3**a,b show typical FLID maps of a pure BC-blinking QD and a mixture of BC- and Auger-blinking QD respectively. Their
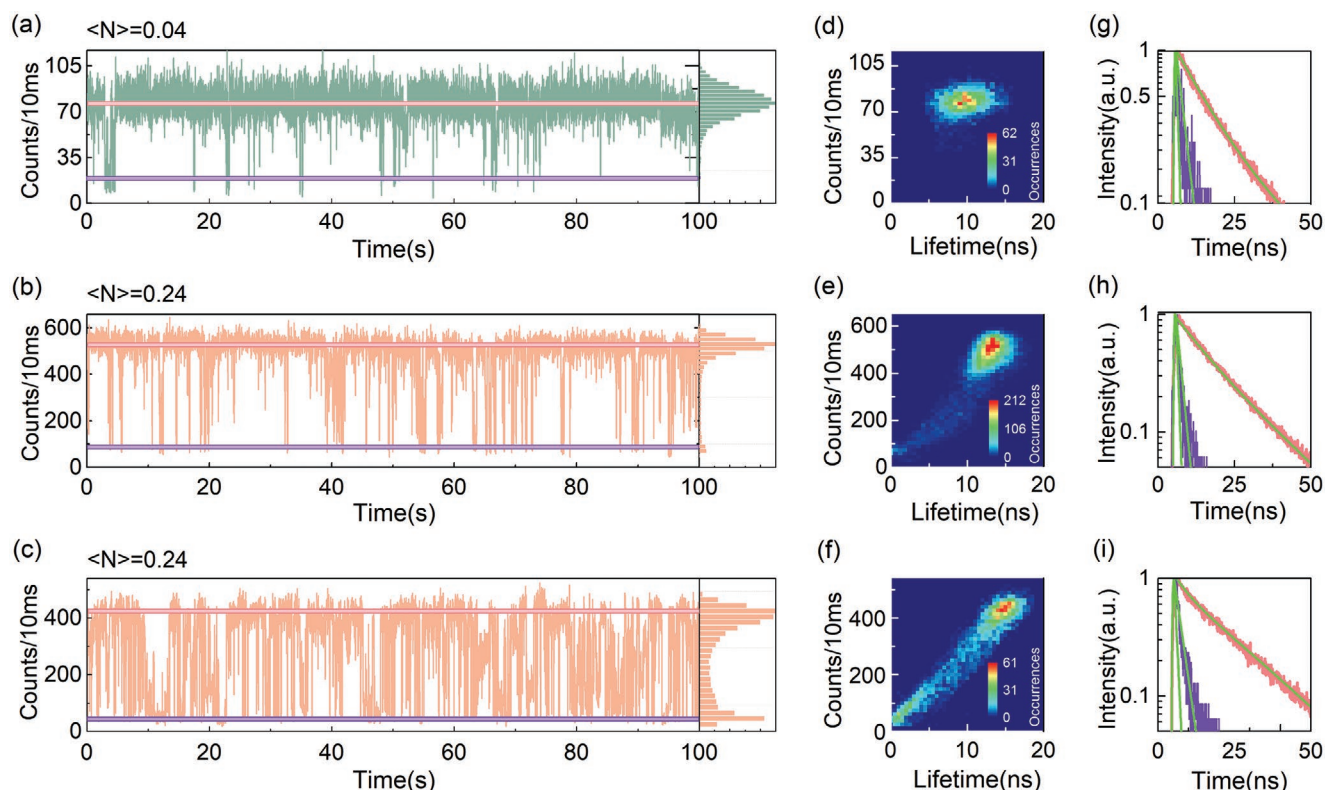
ADVANCED
SCIENCE NEWS
www.advancedsciencenews.com

NANO · MICRO
small
www.small-journal.com

Figure 2. a) A typical PL intensity time trajectory for single $CH_3NH_3PbBr_3$ QDs at $<N> = 0.04$. Corresponding PL intensity histogram on the right panel. b) PL intensity trajectory for the same QD in a) obtained by the excitation of $<N> = 0.24$. c) Typical PL intensity trajectories for some other single QDs at $<N> = 0.24$. d–f) Corresponding FLID maps of the single QDs; color changing from blue to red shows an increase in the probability of occurrence of a given state in intensity-lifetime space. g–i) Corresponding PL decay curves obtained from bright- and dim-state PL regions marked in respective colors on PL intensity histograms of a–c), respectively.
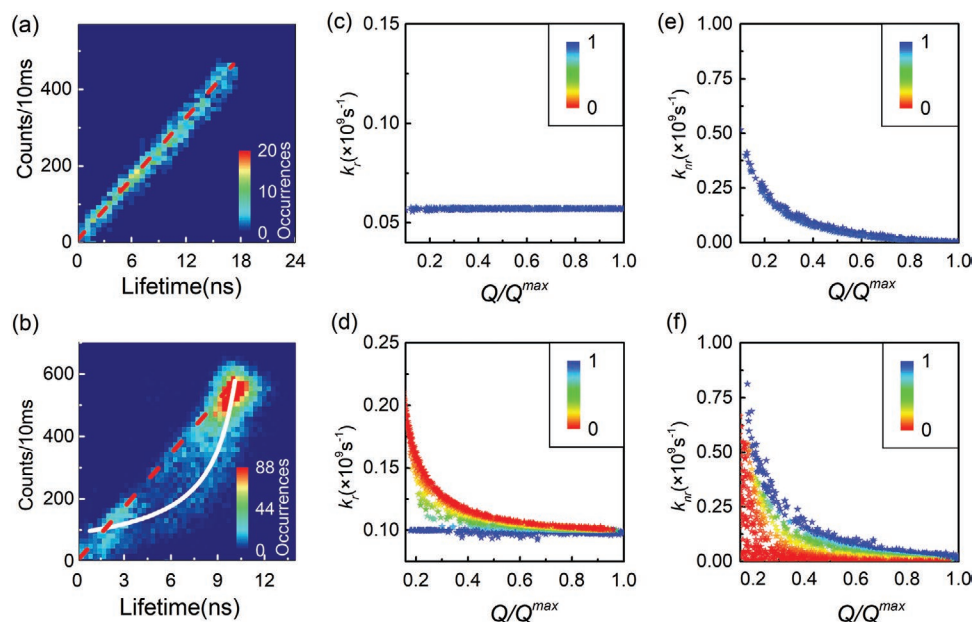

Figure 3. a) Linear FLID map showing a pure BC-blinking. b) Typical FLID map showing a mixture of BC-blinking and Auger-blinking. The BC-blinking and Auger-blinking are indicated by the red dotted line and the white curve. c,d) Corresponding PL quantum yield (QY)-radiative recombination rate (k_r) distribution (PQRD) maps for single QDs in a, b). e,f) Corresponding PQRD maps of nonradiative recombination rate (k_{nr}) for single QDs in a, b). Color changing from blue to red shows a decrease in the proportion of BC-blinking in the PQRD maps.

**ADVANCED
SCIENCE NEWS**

www.advancedsciencenews.com

NANO · MICRO

small

www.small-journal.com

corresponding PQRD maps of k_r are presented in Figure 3c,d, and the corresponding PQRD maps of k_{nr} are presented in Figure 3e,f. The BC-blinking and the Auger-blinking are related to surface trap-induced nonradiative recombination and nonradiative Auger recombination, respectively. Here the proportion of BC-blinking (x) is defined by the ratio of the surface trap-induced non-radiative recombination rate to the total non-radiative recombination rate, while the proportion of Auger-blinking ($1-x$) is defined by the ratio of Auger-induced non-radiative recombination rate to the total non-radiative recombination rate. The color scale from blue to red in the PQRD maps represents that the proportion of BC-blinking decreases while that of Auger-blinking increases. For the pure BC-blinking in Figure 3a, the k_r remains constant (Figure 3c), while the k_{nr} changes constantly with Q/Q^{max} because of the stochastic activation and deactivation of MRCs (Figure 3e).

Because of the absence of pure Auger-blinking in the QDs in our experiments, we present the PQRD maps for pure Auger-blinking in a single CdSe-based QD as an example reference in Figure S1. By comparing them, we can clearly see two types of blinking behaviors are different in their the PQRD maps. Actually, the PQRD maps can clearly separate the contributions of BC- and Auger-blinking in the mixed blinking behavior, as shown in Figure 3d,f. The blue areas originate from BC-blinking, while the red areas originate from Auger-blinking. In Figure 3d, k_r in BC-blinking remains constant, while k_r in Auger-blinking gradually increases from 0.1 to 0.2 with the decreasing Q/Q^{max}, because the radiative rate of the trion state is twice that of a neutral state.[26,51] In Figure 3f, k_{nr} in BC-blinking changes gradually with the increasing Q/Q^{max}, while the k_{nr} in Auger-blinking changes rapidly when the trion state starts dominating QD emission.

We find that the PL blinking in Figure 2c is induced by blended mechanisms of BC-blinking and a small portion of Auger-blinking rather than pure BC-blinking (Figure S2, Supporting Information), which is difficult to be uncovered by the methods of the FLID and the scaling of radiative rates. We note that almost all $CH_3NH_3PbBr_3$ perovskite QDs in this study show a blended blinking mechanism under the excitation of $<N> = 0.24$, where $\approx62\%$ of QDs show a weak Auger-dependent blinking behavior, and the remaining $\approx38\%$ QDs show a more pronounced Auger-blinking. When the excitation power is further increased, the proportions of Auger-blinking in the PL intensity trajectories will increase. However, most perovskite QDs will be quenched quickly under very high excitation conditions. The Auger-blinking is due to the ionization and neutralization of QDs, and can be suppressed by suppressing the QDs' ionization. The possible factors affecting the QDs' ionization include the composition, size, and temperature of the QDs, the band offset between the QDs and the surrounding matrix, as well as the laser excitation intensity.[52] According to the exact origin of PL blinking, proper strategies can be used to effectively suppress the PL blinking of perovskite QDs.[53,54] The suppression of PL blinking is beneficial to the PL-based applications, such as light-emitting devices, low-threshold lasing, single-photon sources. In addition, the PQRD maps can well reveal the exciton dynamics of single QDs, such as the evolutions of radiative and non-radiative recombination rates with PL intensity.

2.4. Intrinsic Quantum-Confined Stark Effect (IQCSE)

Interestingly, the IQCSE is also found in the QDs that show more pronounced Auger-blinking, as shown in **Figure 4**.
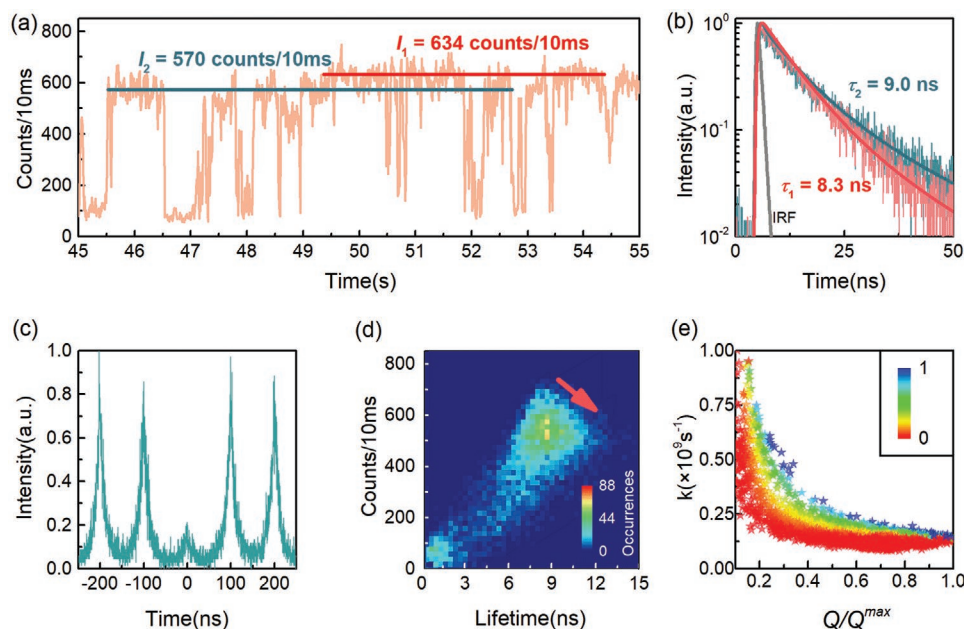

Figure 4. a) A typical PL intensity trajectory for single $CH_3NH_3PbBr_3$ QDs obtained at $<N> = 0.24$. Red line indicates on-state with a normal PL intensity while green line shows on-state with a slightly decreased PL intensity. b) PL decay curves obtained from the PL regions marked by respective colors in (a). c) Corresponding $g^{(2)}$ curve of the single QD. d) Corresponding FLID map. The red arrow represents the changes in the PL intensity and lifetime under the action of IQCSE. e) Corresponding PQRD maps of total recombination rate.
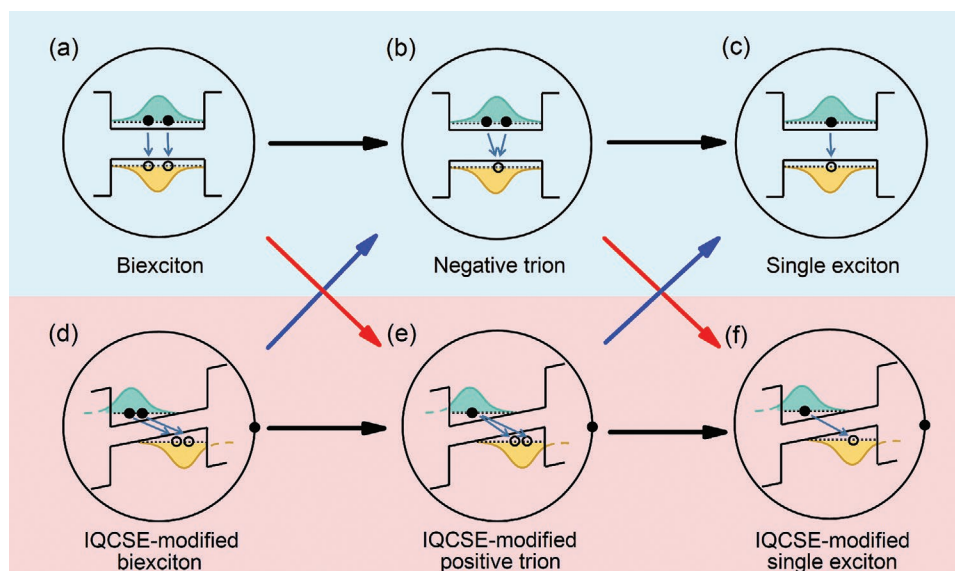
**ADVANCED
SCIENCE NEWS**
www.advancedsciencenews.com

NANO · MICRO
small
www.small-journal.com

Figure 5. Schematic of the generation and elimination of IQCSE. a–c) biexciton, trion, and single exciton states. d–f) IQCSE-modified biexciton, trion, and single exciton states. The red and blue arrows show Auger-induced generation and elimination of IQCSE, respectively. The black arrows show that Auger process makes no contribution to the IQCSE.

A typical PL intensity trajectory from 45 to 55 s for single perovskite QDs is obtained at $<N> = 0.24$ (Figure 4a), which is extracted from the PL trajectory in Figure S3, Supporting Information. Note that the bright-state has several PL-intensity levels, and the PL intensity switches repeatedly between these levels. The red and green lines indicate two different intensity levels of the bright state ($I_1 = 634$ counts/10 ms, $I_2 = 570$ counts/10 ms). Figure 4b shows the corresponding PL decay curves for the two PL intensity levels with respective colors. The decay curves are well-fitted by bi-exponential functions of $A_1 e^{-t/\tau_1} + A_2 e^{-t/\tau_2}$ with 8.80 and 0.22 ns for I_1, and 9.72 and 0.32 ns for I_2. The PL lifetime increases slightly from 8.80 ns to 9.72 ns as the PL intensity decreases from I_1 (634 counts/10 ms) to I_2 (570 counts/10 ms). We attribute this unusual phenomenon to IQCSE, which has also been previously reported for single CdSe-based QDs.[39] Therein, 8.80 ns is attributed to the single exciton lifetime (Figure S4, Supporting Information). By combining single exciton lifetime (τ_X) and $g^{(2)}$ curve (Figure 4c), the lifetime of 0.22 ns satisfies $g^{(2)}(0) \approx Q_{XX}/Q_X = \beta \times \tau_{XX}/\tau_X$ with $\beta \approx 4.0$.[23,55] Therefore, the lifetime of 0.22 ns can be attributed to the lifetime of biexciton. We attribute the prolonged lifetimes (9.72 and 0.32 ns) to IQCSE-modified single exciton and bi-exciton lifetimes. Therefore, the reduced PL intensity and the corresponding prolonged lifetime can confirm the presence of IQCSE in single $CH_3NH_3PbBr_3$ QDs.

The Auger process is correlated with the observed IQCSE in the QDs. The corresponding FLID map is given in Figure 4d. The red arrow indicates that the on-state PL intensity decrease from 680 to 490 counts/10 ms, while the corresponding PL lifetime increase from 8.3 to 11.5 ns due to the IQCSE. Figure 4e shows the corresponding PQRD maps of the total recombination rate for the whole PL trajectory. The red area with a large proportion indicates that Auger-blinking plays a major role in this QD. For QDs with pure BC-blinking in Figure 4a, however, we cannot find any sign of IQCSE. Therefore, our observations

reveal a strong correlation between the Auger process and IQCSE in the perovskite QDs. We propose that the surface charges, which induced the IQCSE, should originate from or be associated with the Auger process.

Hereafter, we propose an Auger-induced IQCSE model to explain the observed IQCSE and its evolvement, as depicted schematically in **Figure 5**. There are six exciton states, including normal (IQCSE-modified) bi-excitons, trions, and single excitons, where the IQCSE is induced by a negative charge for instance. When a bi-exciton state is generated under the photon excitation (Figure 5a), the non-radiative Auger recombination process, acting as a dominant decay channel for the biexciton state, transfers the bi-exciton recombination energy to one of the two extra charge carriers, instead of emitting a photon.[56] The extra carrier could be ejected out of the QD after receiving the bi-exciton recombination energy, forming a trion state inside the QD under the constant photon excitation (Figure 5b).[57] The similar process happens not only from bi-exciton state to the trion state, but also from the trion state to the single exciton state, as indicated by the black arrows. In other cases, the extra carrier that receives the bi-exciton recombination energy is likely to be captured by surface states,[31] as indicated by the red arrows between Figure 5a,e, and then the surface charge induces the IQCSE (the similar process also happens from Figure 5b,f). In this case, the energy band structure of QDs is distorted due to the surface charge, resulting in a reduced overlap of the electron and hole wave functions, which ultimately results in a decreased PL intensity and a prolonged PL lifetime. When the surface electron tunnels back to the QD, it recombines with a confined hole[58,59] and eliminates the IQCSE, as indicated by the blue arrows in Figure 5.

Due to the larger dipole moment of the organic cation $CH_3NH_3^+$ (2.3 D)[60,61] than that of Cs^+, the $CH_3NH_3PbBr_3$ QDs are more sensitive to the external electric field. This has enabled the potential applications of the quantum-confined

**ADVANCED
SCIENCE NEWS**

www.advancedsciencenews.com

**NANO · MICRO
small**

www.small-journal.com

Stark effect in field-controlled electro-optic modulators, sensors, electro-absorption modulators.[60,62,63] Nevertheless, the $CH_3NH_3PbBr_3$ QDs have a more considerable spectral diffusion due to the larger IQCSE, which hinders the related applications. Our research reveals that IQCSE is related to the Auger recombination process. Hence, we can conclude that spectral diffusion can be effectively suppressed by suppressing the Auger process of the QDs. It is worth mentioning that the suppression of spectral broadening in the ensemble level has been recently demonstrated in Auger process-inhibited CdSe/CdS QDs.[64] Proper post-synthetic surface treatments and doping techniques have also been used to effectively suppress the Auger recombination of perovskite QDs.[53,54] In addition, reducing the IQCSE can improve the measurement accuracy of the quantum-confined Stark effect-based devices including field-controlled electro-optic modulators, sensors, electro-absorption modulators.

3. Conclusion

In conclusion, we developed and demonstrated the PQRD method in investigation of the blinking mechanisms and the IQCSE in single organic-inorganic hybrid $CH_3NH_3PbBr_3$ perovskite QDs. The PQRD maps reveal the evolutions of radiative and nonradiative recombination rates with PL intensity and to determine PL blinking mechanisms as well as their respective contributions. The results show that most single QDs exhibit BC-blinking under a low excitation photon fluence, and different proportions of Auger-blinking participate in their PL intensity trajectories under a higher excitation photon fluence. A significant IQCSE has been revealed in single $CH_3NH_3PbBr_3$ QDs, which is strongly related to the Auger recombination process. The Auger-induced IQCSE model is proposed to depict the generation and elimination of IQCSE schematically. These investigations contribute to the rational design of perovskite QDs for applications.

4. Experimental Section

Materials: Methylamine hydrobromide (CH_3NH_3Br, >98.0%(N)(T)), lead bromide ($PbBr_2$, 99.0%), *N,N*-dimethylformamide (DMF, 99.8%), oleic acid (≥99.0%, GC), *n*-octylamine (99%), and acetonitrile (≥99.9%) were purchased from Aladdin. Polystyrene and toluene (≥99.5%) were purchased from Sigma-Aldrich. They were used as received without further purification.

$CH_3NH_3PbBr_3$ Perovskite QDs Synthesis and Characterization: The $CH_3NH_3PbBr_3$ QDs were synthesized as follows. Solution A and solution B, acting as the "aqueous phase", were obtained by 0.16 mmol CH_3NH_3Br dissolved in 0.3 mL DMF, 0.2 mmol $PbBr_2$ dissolved in 0.5 mL DMF, respectively. Solution C, acting as the "oil phase", was the mixture of 10 mL toluene, 0.5 mL oleic acid, and 20 µL n-octylamine. Then the solution A and the solution B were added dropwise into solution C to form an emulsion. Afterward, 8 mL acetonitrile was used as a demulsifier and added dropwise into the emulsion to initiate a demulsion process. By centrifugation at 6000 rpm for 5 min, polar solvents and excess reactants were discarded as supernatant. Then the precipitates were redissolved into 3 mL toluene. After another centrifugation at 5000 rpm for 5 min, larger-sized side-products were precipitated out of the system, and $CH_3NH_3PbBr_3$ QDs in toluene were obtained for further analysis. For single QD measurements, the toluene solution of QDs was mixed with 1 wt.% polystyrene solution to isolate and protect the particles. The mixture was then spin-coated onto clean glass coverslips with a rotation speed of 3000 rpm for 1 min.

The diameter of QDs was measured from the TEM image using a JEM-2100 microscope. The absorption and PL emission spectra of the QDs in toluene were measured on a PerkinElmer Lambda 950 UV–VIS–NIR spectrometer and a Cary Eclipse Fluorescence Spectrophotometer, respectively.

Single-Dot PL Spectroscopic Measurements: A home-made confocal fluorescence imaging microscope was applied to collect the PL photons of single QDs. A 436 nm pulsed laser (EXW-12, NKT, 50–100 ps, 10 MHz repetition rate) was used to excite the QD samples. An oil immersion objective (Olympus, 100×, 1.3 NA) was used not only to focus a laser beam onto the QDs sample but also to collect PL simultaneously. The PL, which passes through a dichroic mirror (Semrock) and a high-pass filter (Semrock), was focused on a 100 µm pinhole to reject photons which were out of focus. Then a 50/50 beam-splitter cube was used to split the PL photons into two beams, which were finally detected by a pair of single-photon avalanche diode detectors (SPCM-AQR-15, PerkinElmer) and recorded by a TTTR-TCSPC data acquisition card (HydraHarp 400, PicoQuant) with a temporal resolution of 16 ps. All measurements were performed at room temperature. The resolution of the confocal imaging microscope was limited to about 300 nm laterally, due to the diffraction limit of light. Therefore, the confocal images of perovskite QDs (Figure 1c) were much larger than their TEM images (Figure 1a).

Supporting Information

Supporting Information is available from the Wiley Online Library or from the author.

Acknowledgements

Conflict of Interest

The authors declare no conflict of interest.

Keywords

[1] H. Huang, M. I. Bodnarchuk, S. V. Kershaw, M. V. Kovalenko, A. L. Rogach, *ACS Energy Lett.* **2017**, *2*, 2071.

[2] Q. A. Akkerman, G. Raino, M. V. Kovalenko, L. Manna, *Nat. Mater.* **2018**, *17*, 394.

[3] B. Li, R. Chen, C. Qin, C. Yang, W. Guo, X. Han, Y. Gao, G. Zhang, L. Xiao, S. Jia, *Appl. Phys. Express* **2019**, *12*, 112003.

[4] X. Chen, F. Zhang, Y. Ge, L. Shi, S. Huang, J. Tang, Z. Lv, L. Zhang, B. Zou, H. Zhong, *Adv. Funct. Mater.* **2018**, *28*, 1706567.

ADVANCED
SCIENCE NEWS
www.advancedsciencenews.com

NANO · MICRO
small
www.small-journal.com

[5] Y. Xu, Q. Chen, C. Zhang, R. Wang, H. Wu, X. Zhang, G. Xing, W. W. Yu, X. Wang, Y. Zhang, M. Xiao, *J. Am. Chem. Soc.* **2016**, *138*, 3761.

[6] S. Chang, Z. Bai, H. Zhong, *Adv. Opt. Mater.* **2018**, *6*, 1800380.

[7] Y. S. Park, S. J. Guo, N. S. Makarov, V. I. Klimov, *ACS Nano* **2015**, *9*, 10386.

[8] H. Wu, Z. Kang, Z. Zhang, Z. Zhang, H. Si, Q. Liao, S. Zhang, J. Wu, X. Zhang, Y. Zhang, *Adv. Funct. Mater.* **2018**, *28*, 1802015.

[9] H. Wu, H. Si, Z. Zhang, Z. Kang, P. Wu, L. Zhou, S. Zhang, Z. Zhang, Q. Liao, Y. Zhang, *Adv. Sci.* **2018**, *5*, 1801219.

[10] H. Wu, Z. Kang, Z. Zhang, H. Si, S. Zhang, Z. Zhang, Q. Liao, Y. Zhang, *Small Methods* **2019**, *3*, 1900117.

[11] P. Lu, M. Lu, H. Wang, N. Sui, Z. Shi, W. W. Yu, Y. Zhang, *InfoMat* **2019**, *1*, 430.

[12] J. Chen, W. Du, J. Shi, M. Li, Y. Wang, Q. Zhang, X. Liu, *InfoMat* **2020**, *2*, 170.

[13] H. Yuan, E. Debroye, G. Caliandro, K. P. Janssen, J. van Loon, C. E. Kirschhock, J. A. Martens, J. Hofkens, M. B. Roeffaers, *ACS Omega* **2016**, *1*, 148.

[14] L. Chouhan, S. Ghimire, V. Biju, *Angew. Chem., Int. Ed.* **2019**, *58*, 4875.

[15] Y. X. Tian, A. Merdasa, M. Peter, M. Abdellah, K. B. Zheng, C. S. Ponseca, T. Pullerits, A. Yartsev, V. Sundstrom, I. G. Scheblykin, *Nano Lett.* **2015**, *15*, 1603.

[16] S. Ghimire, V. Biju, *J. Photochem. Photobiol., C* **2018**, *34*, 137.

[17] M. Gerhard, B. Louis, R. Camacho, A. Merdasa, J. Li, A. Kiligaridis, A. Dobrovolsky, J. Hofkens, I. G. Scheblykin, *Nat. Commun.* **2019**, *10*, 1698.

[18] H. Yuan, E. Debroye, E. Bladt, G. Lu, M. Keshavarz, K. P. F. Janssen, M. B. J. Roeffaers, S. Bals, E. H. Sargent, J. Hofkens, *Adv. Mater.* **2018**, *30*, 1705494.

[19] F. R. Hu, C. Y. Yin, H. C. Zhang, C. Sun, W. W. Yu, C. F. Zhang, X. Y. Wang, Y. Zhang, M. Xiao, *Nano Lett.* **2016**, *16*, 6425.

[20] V. I. Klimov, *Annu. Rev. Phys. Chem.* **2007**, *58*, 635.

[21] Z. J. Li, G. F. Zhang, B. Li, R. Y. Chen, C. B. Qin, Y. Gao, L. T. Xiao, S. T. Jia, *Appl. Phys. Lett.* **2017**, *111*, 153106.

[22] G. Yuan, C. Ritchie, M. Ritter, S. Murphy, D. E. Gómez, P. Mulvaney, *J. Phys. Chem. C* **2018**, *122*, 13407.

[23] B. Li, H. Huang, G. Zhang, C. Yang, W. Guo, R. Chen, C. Qin, Y. Gao, V. P. Biju, A. L. Rogach, L. Xiao, S. Jia, *J. Phys. Chem. Lett.* **2018**, *9*, 6934.

[24] P. A. Frantsuzov, S. Volkan-Kacso, B. Janko, *Phys. Rev. Lett.* **2009**, *103*, 207402.

[25] T. Kim, S. I. Jung, S. Ham, H. Chung, D. Kim, *Small* **2019**, *15*, 1900355.

[26] G. Yuan, D. E. Gómez, N. Kirkwood, K. Boldt, P. Mulvaney, *ACS Nano* **2018**, *12*, 3397.

[27] C. T. Trinh, D. N. Minh, K. J. Ahn, Y. Kang, K. G. Lee, *ACS Photonics* **2018**, *5*, 4937.

[28] C. T. Trinh, D. N. Minh, K. J. Ahn, Y. Kang, K. G. Lee, *Sci. Rep.* **2020**, *10*, 2172.

[29] S. A. Empedocles, D. J. Norris, M. G. Bawendi, *Phys. Rev. Lett.* **1996**, *77*, 3873.

[30] S. Ham, H. Chung, T. W. Kim, J. Kim, D. Kim, *Nanoscale* **2018**, *10*, 2207.

[31] M. G. B. S. A. Empedocles, *Science* **1997**, 2114.

[32] S. H. Lohmann, C. Strelow, A. Mews, T. Kippe, *ACS Nano* **2017**, *11*, 12185.

[33] D. A. B. Miller, D. S. Chemla, T. C. Damen, A. C. Gossard, W. Wiegmann, T. H. Wood, C. A. Burrus, *Phys. Rev. B* **1985**, *32*, 1043.

[34] M. J. Fernee, T. Plakhotnik, Y. Louyer, B. N. Littleton, C. Potzner, P. Tamarat, P. Mulvaney, B. Lounis, *J. Phys. Chem. Lett.* **2012**, *3*, 1716.

[35] G. F. Zhang, Y. G. Peng, H. Q. Xie, B. Li, Z. J. Li, C. G. Yang, W. L. Guo, C. B. Qin, R. Y. Chen, Y. Gao, Y. J. Zheng, L. T. Xiao, S. T. Jia, *Front. Phys.* **2019**, *14*, 23605.

[36] G. F. Zhang, C. G. Yang, Y. Ge, Y. G. Peng, R. Y. Chen, C. B. Qin, Y. Gao, L. Zhang, H. Z. Zhong, Y. J. Zheng, L. T. Xiao, S. T. Jia, *Front. Phys.* **2019**, *14*, 63601.

[37] D. Braam, A. Mölleken, G. M. Prinz, C. Notthoff, M. Geller, A. Lorke, *Phys. Rev. B* **2013**, *88*, 125302.

[38] J. Müller, J. M. Lupton, A. L. Rogach, J. Feldmann, D. V. Talapin, H. Weller, *Phys. Rev. B* **2005**, *72*, 205339.

[39] T. Ihara, Y. Kanemitsu, *Phys. Rev. B* **2014**, *90*, 195302.

[40] J. Gong, M. Yang, X. Ma, R. D. Schaller, G. Liu, L. Kong, Y. Yang, M. C. Beard, M. Lesslie, Y. Dai, B. Huang, K. Zhu, T. Xu, *J. Phys. Chem. Lett.* **2016**, *7*, 2879.

[41] W. G. Lu, C. Chen, D. B. Han, L. H. Yao, J. B. Han, H. Z. Zhong, Y. T. Wang, *Adv. Opt. Mater.* **2016**, *4*, 1732.

[42] G. E. Eperon, E. Jedlicka, D. S. Ginger, *J. Phys. Chem. Lett.* **2018**, *9*, 104.

[43] B. Li, G. F. Zhang, C. G. Yang, Z. J. Li, R. Y. Chen, C. B. Qin, Y. Gao, H. Huang, L. T. Xiao, S. T. Jia, *Opt. Express* **2018**, *26*, 4674.

[44] C. G. Yang, G. F. Zhang, L. H. Feng, B. Li, Z. J. Li, R. Y. Chen, C. B. Qin, Y. Gao, L. T. Xiao, S. T. Jia, *Opt. Express* **2018**, *26*, 11889.

[45] H. Huang, F. Zhao, L. Liu, F. Zhang, X. G. Wu, L. Shi, B. Zou, Q. Pei, H. Zhong, *ACS Appl. Mater. Interfaces* **2015**, *7*, 28128.

[46] B. Li, G. F. Zhang, Z. Wang, Z. J. Li, R. Y. Chen, C. B. Qin, Y. Gao, L. T. Xiao, S. T. Jia, *Sci. Rep.* **2016**, *6*, 32662.

[47] N. Yarita, H. Tahara, T. Ihara, T. Kawawaki, R. Sato, M. Saruyama, T. Teranishi, Y. Kanemitsu, *J. Phys. Chem. Lett.* **2017**, *8*, 1413.

[48] J. A. Castaneda, G. Nagamine, E. Yassitepe, L. G. Bonato, O. Voznyy, S. Hoogland, A. F. Nogueira, E. H. Sargent, C. H. B. Cruz, L. A. Padilha, *ACS Nano* **2016**, *10*, 8603.

[49] G. Nair, J. Zhao, M. G. Bawendi, *Nano Lett.* **2011**, *11*, 1136.

[50] P. P. Jha, P. Guyot-Sionnest, *J. Am. Chem. Soc.* **2009**, *3*, 1011.

[51] Y. S. Park, W. K. Bae, J. M. Pietryga, V. I. Klimov, *ACS Nano* **2014**, *8*, 7288.

[52] A. L. Efros, D. J. Nesbitt, *Nat. Nanotechnol.* **2016**, *11*, 661.

[53] S. Nakahara, H. Tahara, G. Yumoto, T. Kawawaki, M. Saruyama, R. Sato, T. Teranishi, Y. Kanemitsu, *J. Phys. Chem. C* **2018**, *122*, 22188.

[54] N. Mondal, A. De, A. Samanta, *J. Phys. Chem. Lett.* **2018**, *9*, 3673.

[55] X. N. Huang, Q. F. Xu, C. F. Zhang, X. Y. Wang, M. Xiao, *Nano Lett.* **2016**, *16*, 2492.

[56] V. I. Klimov, A. A. Mikhailovsky, D. W. McBranch, C. A. Leatherdale, M. G. Bawendi, *Science* **2000**, *287*, 1011.

[57] C. Galland, Y. Ghosh, A. Steinbrueck, J. A. Hollingsworth, H. Htoon, V. I. Klimov, *Nat. Commun.* **2012**, *3*, 908.

[58] A. Marchioro, P. J. Whitham, K. E. Knowles, T. B. Kilburn, P. J. Reid, D. R. Gamelin, *J. Phys. Chem. C* **2016**, *120*, 27040.

[59] J. Tang, F. Li, G. Yang, Y. Ge, Z. Li, Z. Xia, H. Shen, H. Zhong, *Adv. Opt. Mater.* **2019**, *7*, 1801687.

[60] G. Walters, M. Wei, O. Voznyy, R. Quintero-Bermudez, A. Kiani, D. M. Smilgies, R. Munir, A. Amassian, S. Hoogland, E. Sargent, *Nat. Commun.* **2018**, *9*, 4214.

[61] J. M. Frost, K. T. Butler, F. Brivio, C. H. Hendon, M. van Schilfgaarde, A. Walsh, *Nano Lett.* **2014**, *14*, 2584.

[62] W. Mao, J. Zheng, Y. Zhang, A. S. R. Chesman, Q. Ou, J. Hicks, F. Li, Z. Wang, B. Graystone, T. D. M. Bell, M. U. Rothmann, N. W. Duffy, L. Spiccia, Y. B. Cheng, Q. Bao, U. Bach, *Angew. Chem., Int. Ed.* **2017**, *56*, 12486.

[63] Z. Wang, J. Liu, Z. Q. Xu, Y. Xue, L. Jiang, J. Song, F. Huang, Y. Wang, Y. L. Zhong, Y. Zhang, Y. B. Cheng, Q. Bao, *Nanoscale* **2016**, *8*, 6258.

[64] L. Zhang, B. Lv, H. Yang, R. Xu, X. Wang, M. Xiao, Y. Cui, J. Zhang, *Nanoscale* **2019**, *11*, 12619.